

A Numerical Simulation Study of the Wasabizawa-Akinomiya Geothermal Field, Akita Prefecture, Japan

**Shigetaka Nakanishi¹, John W. Pritchett², Sabodh K. Garg², Chitoshi Akasaka¹,
Shigeo Tezuka³ and Koji Kitao⁴**

¹**Electric Power Development Co. Ltd. (J-Power), Tokyo, Japan**

²**Leidos Inc., San Diego, CA, USA**

³**Yuzawa Geothermal Power Corporation (YGP), Yuzawa, Akita Pref., Japan**

⁴**Mitsubishi Materials Corporation (MMC), Tokyo, Japan**

Keywords

Wasabizawa, Akinomiya, Japan, numerical model, natural state, forecasting, MINC, fracture spacing

ABSTRACT

A numerical reservoir model is presented describing the liquid-dominated Wasabizawa-Akinomiya geothermal field, located in northeastern Honshu in Japan. The steady “natural” state of the field was described by an unsteady heat-up calculation of 200,000 years duration which involved a total of 86 trial and error calculations to attain satisfactory matches with observables such as stable reservoir temperatures and pressures. The final natural state model was used to carry out several pressure interference test simulations to verify the model responses to the actual long term flow tests and pressure histories in shut-in observation wells. Next, the model was employed in a series of forecasts to estimate the electrical capacity of the field and to design optimum exploitation strategies. Since the reservoir system consists of a fracture network in basement rocks (granodiorite and schist), the so-called “conductive MINC” formulation was used for these calculations. The results indicate that, using a double-flash steam plant, the Wasabizawa-Akinomiya field can sustain at least 42 MW of electrical generation for more than fifty years.

1. Background

The Japanese New Energy and Industrial Technology Development Organization (NEDO) supported geothermal development promotional surveys (so-called “C” surveys) for the Wasabizawa geothermal area between 1993 and 1997, and for the adjacent Akinomiya area between 1996 and 2000. These areas are located in Akita prefecture, just southwest of the Uenotai geothermal field which has been producing 28.8 MWe of electricity for the grid since 1994. Originally, the Wasabizawa survey was undertaken by Dowa Mining Company (at that

time the operator of the Uenotai power station; Inoue *et al.* (2000), Suzuki *et al.* (2000)) and the Akinomiya survey was performed by JMC Inc. (Kurozumi *et al.* (2000)), but the interests in the Akinomiya area were transferred to MMC in 2004 and the Wasabizawa prospect was transferred to J-Power and MMC in 2008.

Over time, it became evident that Wasabizawa and Akinomiya represent two parts of a single larger geothermal field. As a result, in 2008 J-Power and MMC entered into an agreement to carry out joint studies to examine the feasibility of developing an electrical power project using geofluids from the Wasabizawa-Akinomiya geothermal reservoir. Two exploratory wells (GW-1 and 2) were drilled in 2009 and a production test was carried out in 2010. In parallel with the feasibility study, J-Power, MMC and Mitsubishi Gas Chemical Company, Inc. (MGC) jointly established the Yuzawa Geothermal Power Corporation (YGP) in April 2010 to manage the resource and to accelerate geothermal exploration for both areas in a unified manner. Since then, YGP has been leading the project and carrying out the environmental impact assessment (EIA) procedure required for constructing the new geothermal power station.

This paper presents the results of the numerical simulation study performed to evaluate the electrical capacity of the field and to design optimum exploitation strategies.

2. Conceptual Model

Figure 1 shows the location of exploratory wells in the Wasabizawa-Akinomiya geothermal field. Over 30 exploratory wells have been drilled in the area so far, and the reservoir character is relatively well delineated by extensive exploration. Stable temperature profiles in representative wells are shown in Figure 2, which exhibit conduction-dominated behavior in a low-permeability shallow caprock layer through which heat flows from the underlying convective reservoir upward into the shallow groundwater system. The caprock appears to extend down to depths corresponding to between +200 m ASL and -200 m ASL (“above sea level”) vertical elevation, below which the convection-dominated reservoir is found at temperatures between 280°C and 290°C.

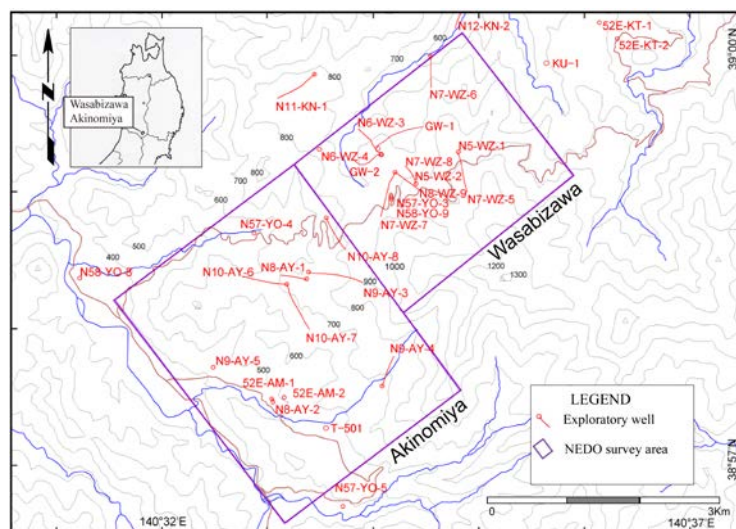


Figure 1: Exploratory well locations in the Wasabizawa-Akinomiya geothermal field. Black: ground surface elevation contours (0.1 kilometer ASL separation).

gas dissolution in the shallow ground water discharge at the Kawarage fumarole area in the north-east where temperatures are relatively low. These facts suggest that the Akinomiya-Wasabizawa reservoir appears to be hydrologically disjoint from the nearby resource supplying the power station at Uenotai.

The volcanic stratigraphy may be subdivided into six major formations. In approximate order of increasing depth, these are: 1. Takamatsudake lava (“*Tk*”), 2. Torakeyama formation (“*Tw*”), 3. Minasegawa formation (“*Mn*”), 4. Ohtoriyazawa formation (“*Ot*”), 5. Doroyu formation (“*Dy*”) and 6. pre-Tertiary basement rocks (“*Bm*”). It is noteworthy that the Wasabizawa-Akinomiya reservoir consists of the fracture network in the pre-Tertiary basement (granodiorite and schist).

3. Development of a Natural-state Model

A three-dimensional, two-phase numerical simulation model of the Wasabizawa-Akinomiya field was developed based on available geological, hydrological, geophysical, geochemical and reservoir engineering data. The model was calibrated by numerous calculations, varying the various unknown parameters (usually permeabilities, sometimes boundary conditions, and occasionally the size/shape of the computational volume) in the model, until a good match was obtained with the natural-state conditions in the reservoir (mainly distributions of pressure, temperature and surface discharge). A total of 86 different natural-state calculations were carried out before an adequate result was obtained. Numerical results discussed hereafter pertain to the final model.

An area measuring 7×8 km in size (56 km²) was selected for numerical simulation using STAR (Pritchett (1995)) as shown in Figure 4. This area incorporates the entire Wasabizawa (7.3 km²) and Akinomiya (11.6 km²) “C” survey areas, and also extends a considerable distance beyond to the northwest, southwest, and southeast. To the northeast, it adjoins the Uenotai geothermal field which is apparently not hydrologically connected to the Wasabizawa-Akinomiya reservoir. The *x*-axis (northeast direction) is subdivided into 24 discrete grid blocks and *y*-axis (northwest direction) is similarly discretized into 22 blocks – the minimum horizontal grid spacing is 0.3 km. Vertically, the *z*-axis was subdivided into 23 layers extending from -2.5 km ASL up to +1.05 km ASL, with 0.10 km grid block spacing above -0.5 km ASL and coarser spacing below. The total number of blocks in the computational grid is (24×22×23 =) 12,144 and the total volume represented is (8 km×7 km × 3.55 km =) 198.8 km³, but it should be noted that not all of these blocks participate in the numerical simulation. Much of the upper part of the computational grid volume lies above the earth surface because of the highly irregular topography. Any grid block whose geometrical center is located at or above the local “water table depth” below the actual local earth surface is reflagged as a “void” grid block and does not participate further in the calculation as representatively indicated in Figure 5. For Case 86 the total number of “void” grid blocks was 2,946, leaving 9,198 blocks that were actually involved in the simulation. The total volume of the “non-void” grid blocks was 166.807 km³.

It is important to realize that not all of this computational volume has been explored by drilling. Of the 29 documented wells located within the 56 km² grid area, most were completed to bottom-hole elevations lying between -0.3 km and -0.9 km ASL (the shallowest – well YO-8 – only reaches +0.358 km ASL and the deepest – well KN-2 – penetrates to -1.172 km ASL), as indicated to the right of Figure 5. As indicated by the figure, which depicts the vertical *x-z*

cross-section at $j = 12$ ($y = 3.45$ km) which has been drilled relatively extensively, about 45% of the volume of the “active” portion of the grid volume is deeper than the bottom-hole location of the deepest well on the field, and is therefore completely unexplored.

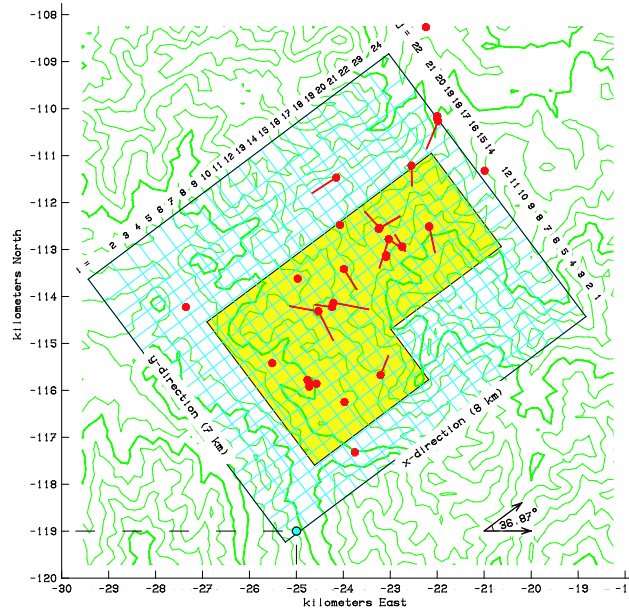


Figure 4: Location of the Wasabizawa-Akinomiya computational grid showing grid orientation and horizontal grid block spacing. Green: ground surface elevation contours (0.1 kilometer RSL separation). Red: locations of existing wells. Cyan: grid block boundaries (0.3 kilometer spacing in central region). Yellow: Akinomiya and Wasabizawa survey areas.

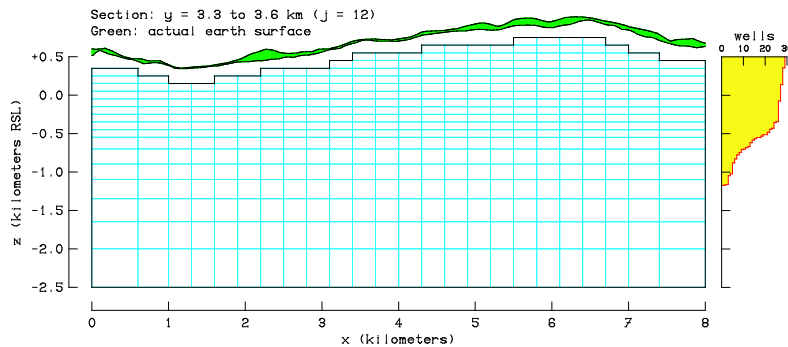


Figure 5: Computational grid viewed in x - z plane at $j = 12$ (3.3 km $\leq y \leq 3.6$ km). Cyan: grid block boundaries. Green: location of earth surface. Yellow: drilling data availability. Note: deepest 45% of grid volume has never been reached by drilling.

To provide conservative estimates of future fluid production capacity, all exterior vertical boundaries of the computational grid volume were treated as impermeable and insulated. The boundary conditions imposed on the bottom surface were subject to a considerable amount of experimentation during the course of the series of calculations that finally led us to Case 86. The experimentation involved changing the elevation of the bottom grid surface, the distribution of basal upward conductive heat flux, and the strength of the upward basal fluid mass flux. The final lower boundary conditions used for Case 86 are indicated in Figure 6. The lower surface is 56 m² in area – most of this surface area (51.86 km², or 92.6%) is treated as impermeable with a fixed distribution of upward conductive heat flux. The conductive heat flux is heterogeneously distributed, with values of 40, 80, 320 and 640 mW/m². The remaining 4.14 km² (7.4%) of the lower grid surface is indicated by the white color in Figure 6 and underlies the Mt. Takamatsu volcano which is believed to be the principal heat source for the geothermal system. In this 4.14 km² area, a uniform fixed upward basal fluid mass flux is imposed that totals 11 kg/s, with fluid inflow temperature 325 °C.

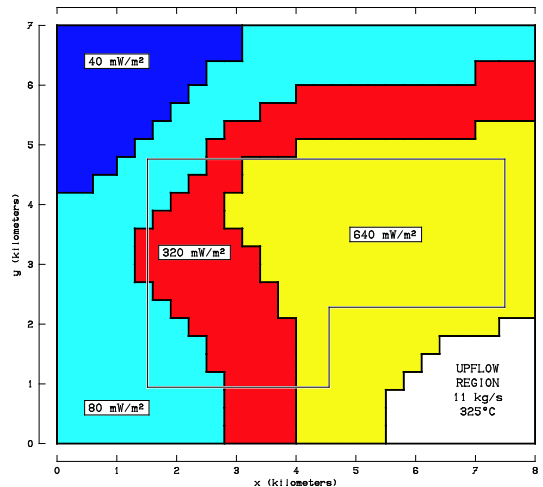


Figure 6: Assignment of boundary conditions along the lower grid surface.

At the upper grid surface, a boundary condition of the “fixed-pressure” type was imposed to allow downward recharge and upward discharge (hot springs etc.) to evolve in a natural fashion. If the mass flux is downward, the inflowing fluid will consist of cold meteoric water (H₂O) unless the flux that is required to maintain the grid block pressure exceeds the available downward meteoric percolation supply. In the latter case, the portion of the downflow requirement that exceeds the available meteoric water supply will consist of atmospheric air (N₂). The available meteoric water supply at the uppermost grid boundary is given by the average annual precipitation (rainfall plus equivalent snowfall) at Wasabizawa, taken as 190 centimeters of precipitation per year or an average annual water flux of 6.025×10^{-5} kg/m²-second, multiplied by a “deep percolation reduction factor” ψ which was taken as equal to 0.125 (1/8) for all cases. Of the total meteoric water supply available, it is therefore being assumed that only 1/8 (*i.e.* 7.53×10^{-6} kg/m²-second) is available for reservoir recharge. As it turns out, in the Case 86 natural-state the maximum value of the downward meteoric recharge flux anywhere on the upper

grid surface was equal to 7.71×10^{-7} kg/m²-s (only about 10% of the above limiting value), so no N₂ ever flows down into the grid.

Rock properties other than permeability (grain density, porosity, heat capacity and thermal conductivity) were fixed in the simulation calculation, and based on measured data for each rock type as shown in Table 1. Available data from drilling in the field clearly indicates that, where formations are permeable, the permeability arises from the presence of fractures that penetrate the otherwise impermeable country rock and provide discrete conduits for fluid flow. Under these circumstances, a conventional “porous- medium” representation may not be appropriate to describe transient phenomena, since this approximation assumes that a state of thermal equilibrium always exists between the solid rock and the fluid flowing through it. In order to deal with the issue (which is, of course, more important for the “forecasting” calculations than for the long-term evolution of the reservoir natural-state), the so-called “conductive MINC” formulation (Pritchett (1997)) was used for all six rock formations to replace the “porous-medium” approximation. Within each computational grid block is a spherical “representative element” consisting of 32 concentric spherical “shells” (31 equal-volume shells representing the impermeable “matrix region” and the outmost shell representing the permeable “fracture zone”), as illustrated in Figure 7. The “fracture zone” porosity is always taken as 50%, so that the volume fraction occupied by the fracture zone (relative to the matrix region) depends on overall porosity. The “average fracture spacing” λ (the diameter of the assembly) is taken to be the same for all grid blocks and equal to 50 meters. The distribution of the absolute permeability (“horizontal permeability” k_h and “vertical permeability” k_z) was established as a part of the “free parameter” variation process during the simulation. The final values assigned for the each rock types are summarized in Figure 8. Figure 9 shows how the various major formation were assigned in the vertical x-z cross-section at $j = 12$ ($y = 3.45$ km).

Table 1: Bulk properties of the various geological formation.

Rock Formation	Grain Density	Overall Porosity	Grain Heat Capacity	Thermal Conductivity
	kg/m ³	%	J/kg-°C	W/m-°C
<i>Tk</i> formation	2300	14	1000	1.7
<i>Tw</i> formation	2500	7	1000	2.1
<i>Mn</i> formation	2500	7	1000	2.1
<i>Ot</i> formation	2600	6	1000	2.4
<i>Dy</i> formation	2600	2	1000	2.4
<i>Bm</i> formation	2700	2	1000	2.4

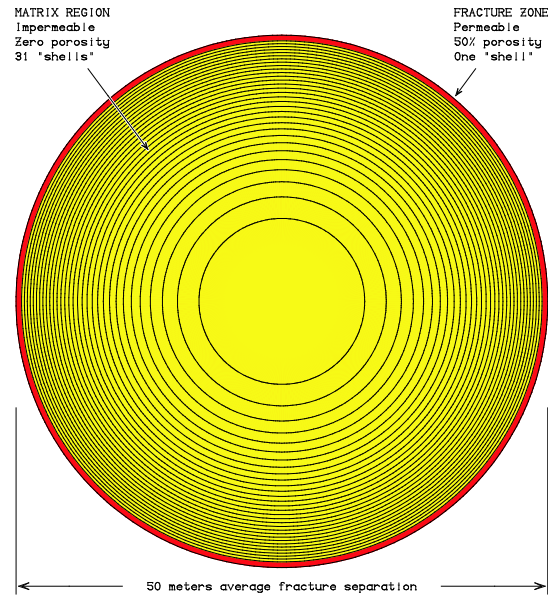


Figure 7: Representative “conductive MINC” assembly used to represent non-equilibrium heat transfer between impermeable country rock matrix and permeable fracture zone for all computational grid blocks. Matrix region (yellow) subdivided into 31 concentric spherical “shells”, each of equal volume, and with zero porosity and zero permeability. Fracture zone (red) represented by single permeable outer shell with 50% porosity. Volume fraction of “fracture zone” varies between 4% and 28% of the volume of the entire spherical assembly (depending on the overall porosity of the rock formation). Diameter of spherical assembly (50 meters) is the “average fracture separation” (λ).

Absolute permeabilities:
 k_h (md) = 0.01 0.10 0.10 2.00 0.20 10.00 1.00
 k_v (md) = 0.02 0.02 0.20 1.00 5.00 5.00 20.00

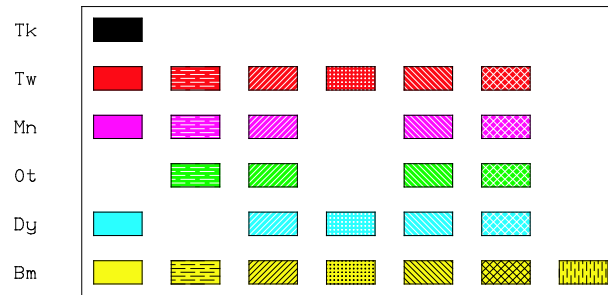


Figure 8: Permeabilities of the various geological formation.

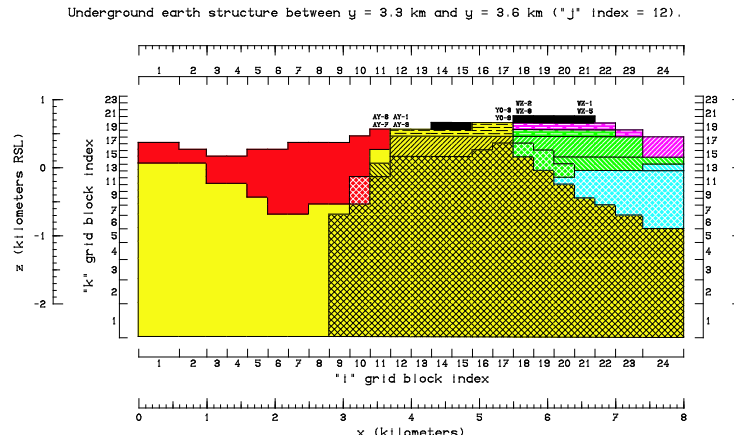


Figure 9: Geological cross-section in x - z plane at $j = 12$. “Key” for interpretation of geological structure is provided in Figure 8.

4. Calculation of the Natural State

Figure 10 shows the change in total grid thermal energy with time (relative to the initial state) during the 200,000 year calculation. After 120,000 years, the thermal energy content of the system is essentially constant, and for practical purposes the final state of the system at $t = 200,000$ years appears to be entirely stable and steady.

Figure 11 shows how the measured stable shut-in feedpoint pressures in the various wells compare with the corresponding pressure values from the 200,000-year Case 86 results, interpolated among principal grid-block pressures to the location of each well’s feedpoint. Considering the probable measurement uncertainty itself, agreement is seen to be reasonably good.

Downhole shut-in temperature profiles from 16 wells which are believed to be reasonably stable and representative of reservoir temperatures were available for comparison with the computed natural-state temperature interpolated among the adjacent grid-block temperatures along the well track. A representative sample of these comparisons is shown on Figure 12. On the whole the computed natural-state temperature distribution appears to be verified by these measured data.

In NEDO’s “C” survey, several pressure interference tests were performed during long-term flow tests using several wells. Although the relatively coarse spatial discretization (minimum block size is $0.3 \text{ km} \times 0.3 \text{ km} \times 0.1 \text{ km}$) may not be ideal for simulating these pressure interference experiments, the model was employed in several pressure interference tests calculations to confirm the model responses to the actual long term flow tests. Figure 13 shows the computed pressure histories compared to the recorded pressure signals (from printed NEDO reports) for which the observation well was located at some distance away from the flowing wells. On the whole the comparison is reasonably satisfactory, particularly in light of the various uncertainties in the measured pressure records.

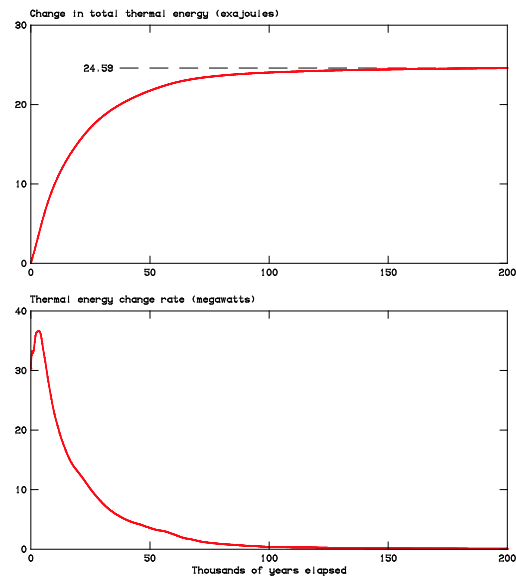


Figure 10: Calculated heat content changes in computational volume over 200,000-year stabilization history. Upper: cumulative total thermal energy change relative to initial conditions. Lower: time-derivative of upper curve. Note: one exajoule = 10^{18} joules.

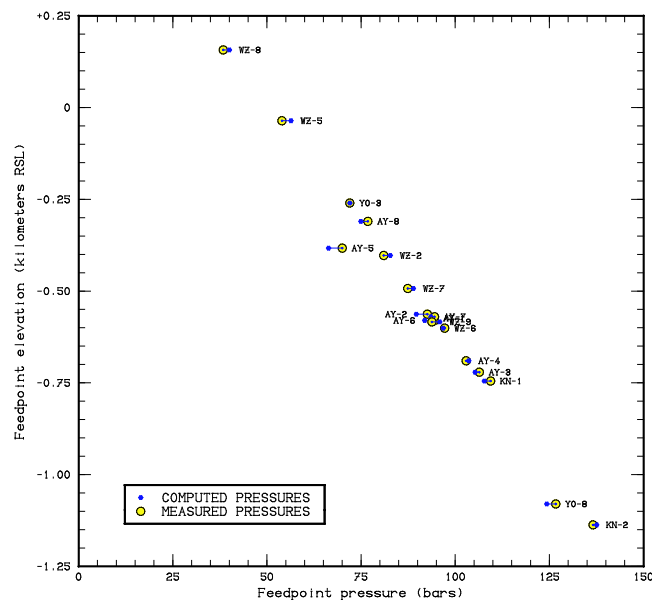


Figure 11: Comparison between measured downhole feedpoint pressures in wells (yellow) and computed natural-state pressures at feedpoint locations (blue) as function of feedpoint elevation.

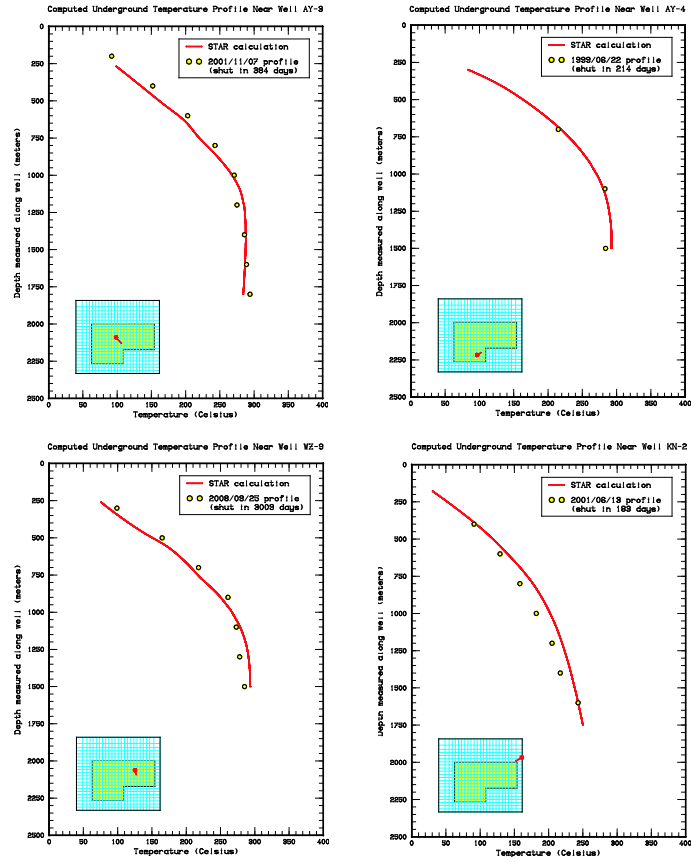


Figure 12: Comparison of stabilized downhole temperatures measured in well AY-3, AY-4, WZ-9 and KN-2 (yellow) with computed natural-state temperatures along well path (red).

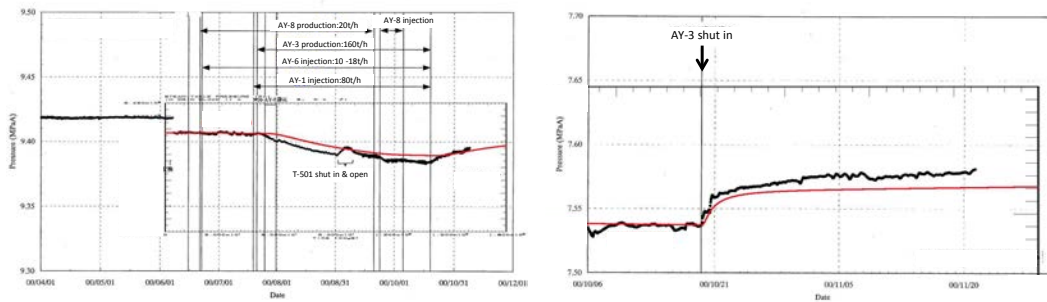


Figure 13: Pressure interference data at well AY-2 (Left) and AY-8 (Right) due to production of well AY-3 and injection to wells AY-1 & 6. Black: measured pressure. Red: calculated pressure.

5. Performance Forecasts

Once a satisfactory representation of the natural state of the reservoir had been developed, we proceeded to carry out a series of parametric forecasts of the probable response to fluid production for electrical power generation. For all of these forecasts, the properties of the rocks and the boundary conditions were maintained the same as in the previous “natural-state” calculation. To simulate the exploitation of the field, additional production and injection wells were incorporated into the model at various locations. The forecast calculations were all carried forward in time from $t = 0$ (*i.e.* the “natural-state” condition) to $t = 50$ years.

Flowing wellhead pressure for all production wells was maintained at or above 8.5 bars. Each production well was assumed to have a time-dependent productivity index given by:

$$PI = V^*/v_{\text{eff}}$$

where V^* is a constant with dimensions of volume, and v_{eff} is the time-dependent effective flowing kinematic viscosity of the (possibly two-phase) fluid mixture in the well’s feed block. The only existing well in the Wasabizawa area for which sufficient data were available to estimate the downhole flowing productivity index was well WZ-9, and the PI was rather low and equal to 0.97 kg/s of fluid discharge per bar of pressure drop. The available measurements for well WZ-9 suggest that, for this well,

$$V^* = 1.2 \times 10^{-12} \text{ m}^3$$

It was assumed that existing well WZ-7 and all “future” production wells at Wasabizawa will have the same V^* value and that all such wells will also have the same inside diameter as WZ-9.

The model operates in “fixed steam flowrate” mode: if, at any instant of time, the capacity of the wellfield to supply steam is insufficient, an additional make-up well is automatically “drilled”. A 30 MWe single-flash steam turbine power station of conventional design was selected for the “Base Case”, with which all other forecast calculations are compared. The fluid flows required from the production wells and the disposal requirements (for both waste separated brine and excess steam condensate) to be met by the injection wells are computed at each instant of time by STAR’s internal “power plant model.”

Figure 14 illustrates the geometry assumed for the Base Case forecast calculation. Fluid is withdrawn from production wells located within the 1.08 km² “Wasabizawa Production Area”, and all fluid reinjection takes place within the “Akinomiya Injection Area” (0.54 km²). The figure also shows the locations of two hypothetical “monitor wells” where changes in pressure at an elevation of -1 km ASL are assumed to be monitored continuously.

Figure 15 shows the comparison between the 30 MWe Base Case and a 45 MWe single-flash forecast in terms of (a) production well drilling requirements, (b) average production well discharge enthalpy, and (c) Wasabizawa monitor well pressure forecast. The 30 MWe Base Case forecast result suggests a sustainable development scenario, but the 45 MWe single-flash case is far less so, mainly because of excessive reservoir pressure decline. The substantial decline in reservoir pressure causes a partial dry-out of the production horizons after about 20 years which results in the rising average discharge enthalpies

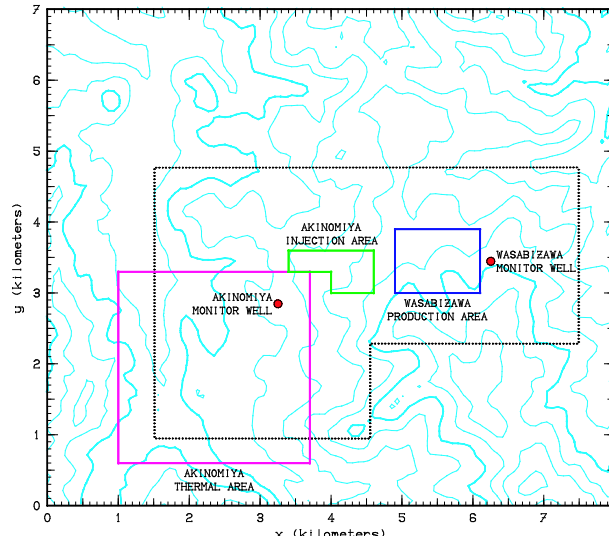


Figure 14: Base Case geometry. Blue: production wellfield area. Green: injection wellfield area. Pink: Akinomiya thermal area. Red: locations of hypothetical deep pressure monitor wells. Cyan: topography contours (contour interval is 0.1 km ASL).

Double-flash plant cases were also studied for 35 MWe and 45 MWe capacity, and both cases suggested sustainable development. Results for the now-planned conventional 42 MWe double-flash plant are also shown in Figure 15. Figure 16 shows the evolution of the temperature distribution at -0.5 km ASL elevation for the final 42 MWe double-flash case. It appears that cold reinjected water from the Akinomiya wellfield will not influence the production enthalpies even after many years of operation.

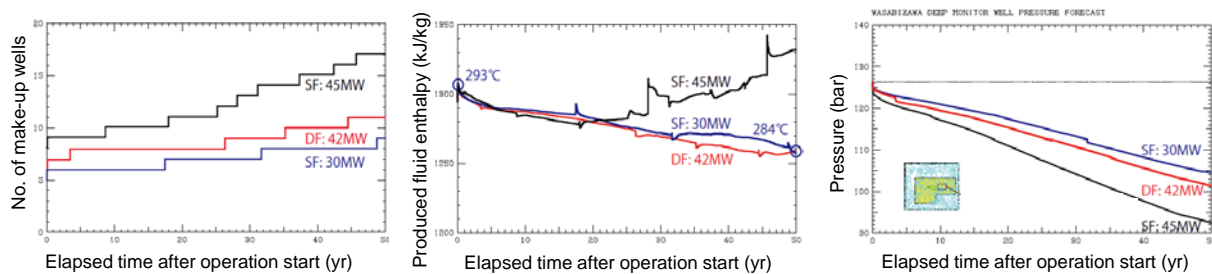


Figure 15: Forecasts of production well drilling requirement (Left), mass-averaged production well discharge enthalpy histories (Center) and pressure changes at -1 km ASL elevation in the hypothetical deep Wasabizawa monitor well (Right) for single-flash 30MWe (Blue), single-flash 45 MWe (Black), and double-flash 42 MWe (Red) plant output.

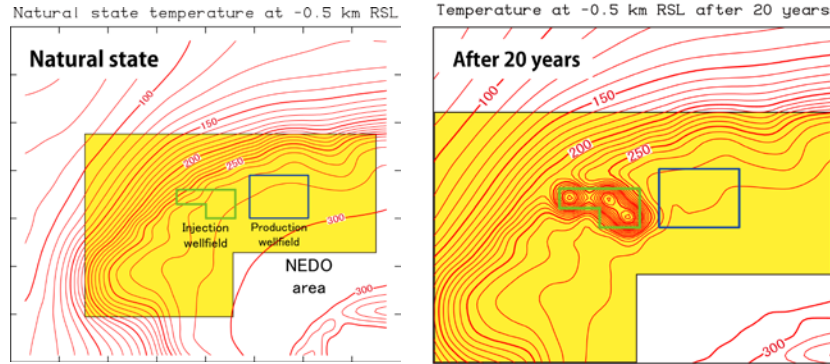


Figure 16: Evolution of temperature distribution at -0.5 km ASL elevation for the double-flash 42 MWe case forecast. Red: temperature contours (spacing is 10°C). Blue: production wellfield. Green: injection wellfield. Left: natural-state temperature. Right: after twenty years of field operation.

Several calculations were carried out to establish the sensitivity of the computed results to certain key assumptions. First, four additional recalculations were carried out using fracture spacing values of $\lambda = 25$ m, 35 m, 70m and 100 m for comparison with the $\lambda = 50$ m “Base Case”. The effect of this fourfold variation in average fracture spacing upon the drilling requirement forecast is fairly small. The reason is that the “Akinomiya injection wellfield” is located far away from the “Wasabizawa production wellfield”, so that the production enthalpies are not apparently affected by cold reinjected water. Other parametric calculations were carried out with each of the production wells (except for well WZ-9 itself) characterized by the same value of V^* , either 0.50, 0.75, 1.5 or 2.0 times the “base case” value ($1.2 \times 10^{-12} \text{ m}^3$). Studies of sensitivity to the cold meteoric recharge limit were also carried out. Various injection schemes were also evaluated, such as pressurized injection with a hybrid cooling system instead of the “base case” scheme (flash-tank, wet cooling tower). These parametric studies helped evaluate the robustness of the model and were thereby useful for project planning and implementation.

6. Concluding Remarks

A numerical model has been constructed for the Wasabizawa-Akinomiya geothermal field which is conservative in character and in good agreement with available measurements from the field. Calculations based upon the model indicate that the field can sustain more than 42 MW of electrical output using a double-flash steam plant for more than fifty years. YGP’s new “Wasabizawa Geothermal Power Station” is now under construction, and commercial operation of the plant will begin in May 2019.

7. Acknowledgements

The authors wish to thank the management of J-Power, MMC, MGC and YGP for the permission to publish this paper. They would also like to thank Tsuneo Ishido of Geological Survey of Japan for his help in carrying out the pressure interference calculations.

REFERENCES

- Inoue, T., Suzuki, M., Yamada, K., Fujita, M., Huzikawa, S., Fujiwara, S., Matsumoto, I., and Kitao, K. "Geological Structure and Subsurface Temperature Distribution in the Wasabizawa Area, Akita Prefecture, Japan." *Proceedings: World Geothermal Congress 2000*, Kyushu-Tohoku, Japan (2000), 2095-2096.
- Kurozumi, H., Kajiwara, T., Suzuki, I., Fukuda, D., Takemoto, S., Yanagiya, S., Ishizuka, Y., Kizaki, A., Takahashi, M., Saeki, K., Tamesue, T., and Ota, H. "Geothermal System in the Akinomiya Area, Northeast Japan." *Proceedings: World Geothermal Congress 2000*, Kyushu-Tohoku, Japan (2000), 1371-1376.
- Pritchett, J. W. "STAR – A Geothermal Reservoir Simulation System" *Proceedings: World Geothermal Congress 1995*, Florence (1995).
- Pritchett, J. W. "Efficient Numerical Simulation of Non-equilibrium Mass and Heat Transfer in Fractured Geothermal Reservoirs." *Proceedings: 22nd Workshop on Geothermal Reservoir Engineering*, Stanford University, Stanford, CA (1997).
- Suzuki, M., Futagoishi, M., Inoue, T., Yamada, K., Obara, K., Fujino, T. "Conceptual Hydrogeological Model of the Wasabizawa Geothermal Field, Akita Prefecture, Japan." *Proceedings: World Geothermal Congress 2000*, Kyushu-Tohoku, Japan (2000), 2241-2245.